AKAP220 manages apical actin networks that coordinate aquaporin-2 location and renal water reabsorption

Jennifer L. Whiting[a,b], Leah Ogier[a,b], Katherine A. Forbush[a,b], Paula Bucko[a,b], Janani Gopalan[b], Ole-Morten Seternes[a,b,1], Lorene K. Langeberg[a,b], and John D. Scott[a,b,2]

[a]Howard Hughes Medical Institute, University of Washington, Seattle, WA 98195; and [b]Department of Pharmacology, University of Washington, Seattle, WA 98195

Edited by Jack E. Dixon, University of California, San Diego, CA, and approved June 6, 2016 (received for review May 13, 2016)

Filtration through the kidney eliminates toxins, manages electrolyte balance, and controls water homeostasis. Reabsorption of water from the luminal fluid of the nephron occurs through aquaporin-2 (AQP2) water pores in principal cells that line the kidney-collecting duct. This vital process is impeded by formation of an "actin barrier" that obstructs the passive transit of AQP2 to the plasma membrane. Bidirectional control of AQP2 trafficking is managed by hormones and signaling enzymes. We have discovered that vasopressin-independent facets of this homeostatic mechanism are under the control of A-Kinase Anchoring Protein 220 (AKAP220; product of the *Akap11* gene). CRISPR/Cas9 gene editing and imaging approaches show that loss of AKAP220 disrupts apical actin networks in organoid cultures. Similar defects are evident in tissue sections from AKAP220-KO mice. Biochemical analysis of AKAP220-null kidney extracts detected reduced levels of active RhoA GTPase, a well-known modulator of the actin cytoskeleton. Fluorescent imaging of kidney sections from these genetically modified mice revealed that RhoA and AQP2 accumulate at the apical surface of the collecting duct. Consequently, these animals are unable to appropriately dilute urine in response to overhydration. We propose that membrane-proximal signaling complexes constrained by AKAP220 impact the actin barrier dynamics and AQP2 trafficking to ensure water homeostasis.

signal transduction | A-Kinase Anchoring Protein | kidney physiology

Human kidneys filter approximately 180 L of fluid every day, yet only approximately 1.5 L of urine is excreted. The majority of this water is reabsorbed from the luminal fluid of the nephron (1). Regulated water reabsorption in response to dehydration occurs through aquaporin-2 (AQP2) water pores in the principal cells of the collecting duct (2). This is stimulated by the hormone arginine vasopressin (AVP). Vasopressin induces PKA phosphorylation of serine 256 on AQP2 and stimulates its translocation from intracellular vesicles to the apical membranes of cells lining the collecting ducts. Reabsorption of water through the kidney preserves fluid balance and results in more concentrated urine (3, 4). Conversely, when an animal ingests excess water, decreased plasma osmolality inhibits vasopressin release, and AQP2 is recovered from the apical membrane by endocytosis. This renders the collecting duct impermeable to water, thereby diverting excess water through the ureter to the bladder.

Not surprisingly, defects in AQP2 trafficking have pathophysiological outcomes. For example, nephrogenic diabetes insipidus (NDI) is associated with impaired vasopressin signaling to AQP2 (5–8). Symptoms include excessive thirst, excretion of a large volume of dilute urine, and electrolyte imbalances, including hypernatremia (1, 5). Hereditary forms of this disease appear in patients with inactivating mutations in the V2 vasopressin receptor (V2R) or AQP2 (9–12). Thus, understanding the molecular mechanisms that govern bidirectional control of AQP2 location may lead to new therapeutic approaches for the treatment of NDI.

Although the enzymes and effector proteins that govern AQP2 internalization remain largely unknown, several studies have emphasized a role for the actin cytoskeleton (13–16). Likewise membrane-proximal complexes of protein kinases and phosphatases impact the reversible control of AQP2 trafficking (17, 18). A-Kinase Anchoring Proteins (AKAPs) that constrain macromolecular complexes of protein kinase A and other signaling enzymes have been implicated in this process (19–22). AKAP220 is a ubiquitously expressed vesicular and membrane-associated anchoring protein of 220 kDa that sequesters several enzymes, including PKA, glycogen synthase kinase-3β (GSK3β), and protein phosphatase 1 (23–26). AKAP220 also interacts with the Rho-family GTPase effector protein IQGAP near the cell cortex to positively regulate actin polymerization and microtubule stability during membrane protrusion and cell migration (27, 28). In the principal cells of the kidney-collecting duct, AKAP220 is also believed to physically associate with AQP2 (22).

In this report, we show that deletion of AKAP220 correlates with inappropriate water reabsorption following overhydration. Cellular and molecular analyses of AKAP220-null mice indicate that elements of this AKAP signaling complex orchestrate "actin barrier" dynamics and trafficking of AQP2 to the apical membranes of kidney-collecting ducts.

Significance

Systemic control of water homeostasis is a vital physiological process. Vasopressin-regulated reabsorption of water through aquaporin-2 (AQP2) water pores in the kidney preserves fluid balance and results in more concentrated urine. We have discovered that the scaffolding protein A-Kinase Anchoring Protein 220 (AKAP220) controls vasopressin-independent aspects of AQP2 trafficking at apical membranes of cells of the kidney-collecting ducts. We postulate that this proceeds via a molecular mechanism that evokes RhoA-mediated modulation of "actin barrier" dynamics. Loss of AKAP220 leads to accumulation of AQP2 at the apical plasma membrane and reduces urine-diluting capacity during overhydration. This phenotype may be clinically relevant, as accumulation of AQP2 at the apical membrane is the desired therapeutic outcome when treating patients with certain renal disorders, including nephrogenic diabetes insipidus.

Author contributions: J.L.W., K.A.F., P.B., O.-M.S., and J.D.S. designed research; J.L.W., L.O., K.A.F., P.B., and O.-M.S. performed research; J.L.W., L.O., K.A.F., P.B., J.G., O.-M.S., L.K.L., and J.D.S. analyzed data; and J.L.W., L.K.L., and J.D.S. wrote the paper.

The authors declare no conflict of interest.

This article is a PNAS Direct Submission.

[1]Present address: Department of Pharmacy, University of Tromsø, The Arctic University of Norway, 9037 Tromsø, Norway.

[2]To whom correspondence should be addressed. Email: scottjdw@uw.edu.

Results

Deletion of AKAP220 Disrupts Apical Actin Networks. AKAP220, a product of the *Akap11* gene, has been implicated in the modulation of cytoskeletal signaling events (23, 28). Microarray analyses detect enhanced expression of the *Akap11* gene in primary cultures of inner medullary collecting duct (IMCD) cells (29). In fact, *Akap11* transcripts are enriched by an order of magnitude over all other AKAP transcripts in these cells. Further support for this notion was provided by immunoblot analysis of mouse kidney lysates (Fig. 1*A*). AKAP220 protein was more prominent in the medulla than the cortex (Fig. 1*A*, *Top*, lane 1). Expression of GAPDH was used as a loading control (Fig. 1*A*, *Bottom*). These findings are consistent with biochemical screens that detected a high molecular weight RII-binding protein in AQP2-containing endosomes from primary murine IMCD cells (19, 30). Because AQP2 is a key constituent of the principal cells of the IMCD, we reasoned that elements of the AKAP220 signaling complex may modulate actin-remodeling events that are required for AQP2 trafficking.

Our next step was to investigate actin organization in mouse IMCD3 (mIMCD3) cells lacking AKAP220. CRISPR/Cas9 gene editing was used to delete the anchoring protein from this immortalized epithelial cell line derived from the mouse inner medullary-collecting duct. Immunoblot analysis confirmed the loss of AKAP220 (Fig. 1*B*, *Top*, lane 2), and GAPDH served as a loading control (Fig. 1*B*, *Bottom*). When grown in Matrigel, mIMCD3 cells form 3D polarized spheroids (31). This offers an elegant model system that is amenable to microscopic analysis of the actin cytoskeleton (31, 32). To determine whether loss of AKAP220 impacts actin organization, spheroids were grown from WT or AKAP220-null cells (Fig. 1 *C*–*I*).

Spheroid samples were fixed in 4% (vol/vol) paraformaldehyde, and F-actin was labeled with Alexa 488-phalloidin before analysis by spinning-disk confocal fluorescence microscopy (Fig. 1 *C* and *D*). WT and AKAP220$^{-/-}$ cells produced polarized spheroids with defined lumena and visible actin networks. Polarized enrichment of F-actin was detected at the apical membrane of WT mIMCD3 spheroids (Fig. 1 *C* and *E*). In contrast, aspects of the actin network were disorganized in AKAP220$^{-/-}$ spheroids. Specifically, a decrease in cortical F-actin was evident near the apical membrane (Fig. 1 *D* and *F*). Other actin-rich structures such as cell junctions were intact in spheroids from both cell lines (Fig. 1 *G* and *H*). The fluorescent intensity of stained F-actin was measured within a 1-μm region of interest (ROI) of the apical

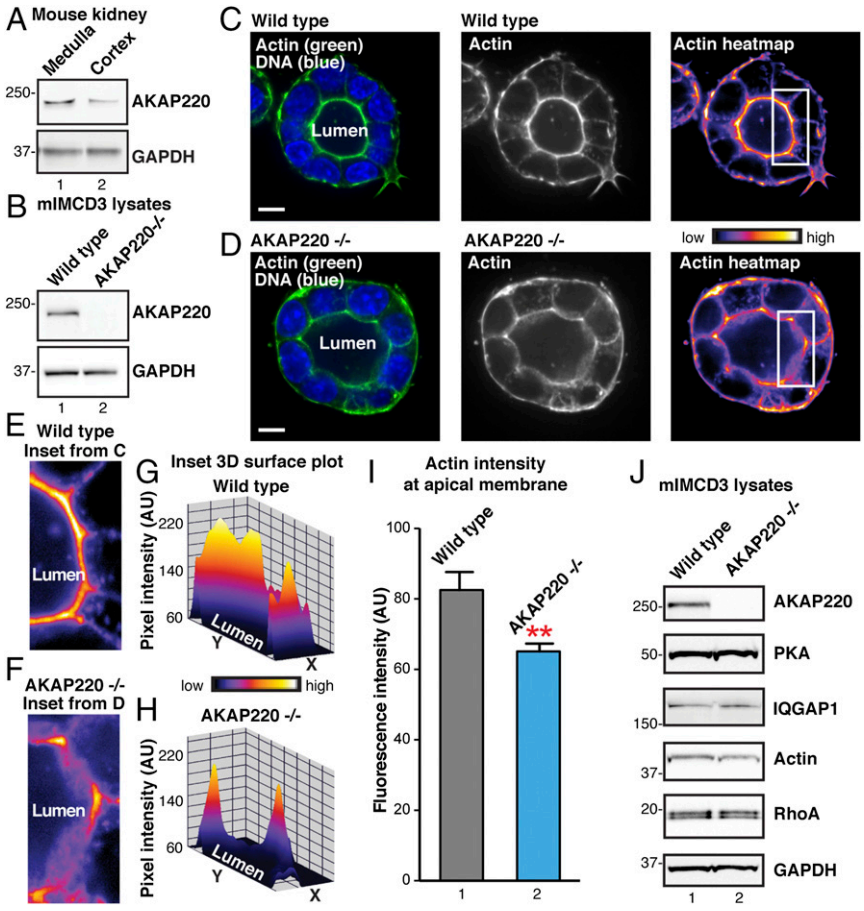

Fig. 1. Deletion of AKAP220 disrupts apical actin structures in mIMCD3 spheroids. (*A*) Western blots of AKAP220 (*Top*) and GAPDH (*Bottom*) in the medulla and cortex of the mouse kidney. (*B*) Western blots of AKAP220 (*Top*) and GAPDH (*Bottom*) in WT and gene-edited AKAP220$^{-/-}$ mIMCD3 cells. (*C* and *D*) Fluorescent staining of F-actin (Alexa 488 phalloidin; green) and DNA (DAPI; blue) in 3D cultured spheroids grown from (*C*) WT or (*D*) AKAP220$^{-/-}$ mIMCD3 (*Left*). (Scale bars: 10 μm.) Lumena are indicated. Accumulation of actin signal at the apical membranes of luminal cells is shown in grayscale (*Middle*) and pseudocolor heat-map images (*Left*). Boxes (*Inset*) indicate ROIs in *E*–*I*. (*E and F*) Magnified heat-map inset images from regions indicated in *C* and *D* highlight actin signal at apical membranes in WT mIMCD3 (*E*) and AKAP220$^{-/-}$ (*F*) spheroids. (*G* and *H*) Heat-map 3D surface plots of insets (*E* and *F*) show differences in F-actin networks at apical membranes of WT and AKAP220$^{-/-}$ spheroids. (*I*) F-actin fluorescence intensity within 1-μm ROI at apical membranes of individual spheroid cells ($n \geq 26$ cells per replicate; $n = 3$ replicate experiments; $P = 0.0025$, unpaired t test). (*J*) Western blot analysis of PKA, IQGAP1, actin, and RhoA in WT mIMCD3 (lane 1) and AKAP220$^{-/-}$ cells (lane 2). GAPDH staining is shown as loading control.

membrane surface in control and AKAP220$^{-/-}$ spheroids (Fig. 1*I*). Cortical actin intensity was significantly reduced at the apical membrane in AKAP220$^{-/-}$ spheroids compared with WT controls ($n \geq 26$ cells; $n = 3$ experiments; representative experiment shown in Fig. 1*I*). Immunoblot analysis confirmed that AKAP220$^{-/-}$ cells express normal levels of PKA, IQGAP1, actin, and RhoA (Fig. 1*J*). Therefore, we conclude that loss of AKAP220 disrupts apical actin remodeling in organoid cultures, but in a manner that does not affect the expression levels of selected AKAP220 binding partners and actin effectors.

Apical actin reorganization is linked to AQP2 trafficking in kidney-collecting ducts (13). When an animal is adequately hydrated, a dense network of actin polymerizes at the apical pole of the principal cells of the collecting duct (13). This actin barrier physically prevents the fusion of AQP2-containing vesicles with the apical plasma membrane. Conversely, upon dehydration and the release of the hormone vasopressin, the actin barrier is depolymerized (4, 33). Thus, water homeostasis requires equilibrium between AQP2 vesicles that are sequestered in the cytoplasm by the actin barrier and active water pores fused to the apical membranes.

Phenotypic Profiling of AKAP220-KO Mice. To further explore the signaling mechanisms that coordinate actin-barrier dynamics, we generated a mouse AKAP220-KO model. LoxP sites were inserted into the *Akap11* gene flanking exons 6 and 7, a region containing 83% of the AKAP220 coding sequence (Fig. 2*A*). Floxed alleles were detected by a 78-bp-size shift in PCR genotyping corresponding to the inserted DNA sequence containing the LoxP site (Fig. 2*B*). Floxed animals were crossed to EIIa-Cre mice, and offspring were genotyped by PCR (Fig. 2*C*). Two primer sets were used to detect the presence of WT, floxed, or collapsed alleles. The colony was backcrossed onto a pure C57BL/6J genetic background for more than seven generations before phenotypic analyses. A Western blot survey of nine tissues revealed that AKAP220 was absent throughout the body (Fig. 2*D*).

Initial profiling of AKAP220-KO mice identified a noticeable decrease in body size (Fig. 3*A*). Total body weight is reduced in males and females (Fig. 3 *B* and *C*). These differences were apparent before weaning and persisted into adulthood (Fig. 3 *B* and *C*). At postnatal day 50 (P50), WT males weighed 23.0 ± 0.5 g ($n = 6$), whereas AKAP220-KO mice weighed 19.7 ± 0.4 g ($n = 8$; $P = 0.0004$, two-tailed *t* test). Likewise, P50 WT females weighed 18.0 ± 0.3 g ($n = 10$), whereas AKAP220-KO females weighed 15.93 ± 0.5 g ($n = 9$; $P = 0.0014$, two-tailed *t* test). This body-weight phenotype correlates with reduced body length (measured from nose to base of tail) and reduced tibia length (Fig. 3 *D* and *E*). However, more rigorous analyses revealed no differences in organ weight of AKAP220-KO mice when normalized body weight of each animal (percentage of total body weight; Fig. 3*F*). The AKAP220-KO mice did not display organ atrophy or hypertrophy that would compound the reduced body-weight phenotype.

Reduced body weight or lean phenotypes can be attributed to changes in basic locomotor behavior such as hyperactivity. Therefore, we used the open-field test to identify any overt changes in locomotor-related behaviors (34, 35). We noted a statistically significant decrease in total distance traveled by AKAP220-KO mice over 30 min compared with WT controls (Fig. 3*G*). AKAP220-KO mice traveled only 7.3 ± 0.5 m ($n = 8$) over the 30-min period, whereas the WT mice traveled a total distance of 11.3 ± 0.6 m ($n = 8$; Fig. 3*H*). The average velocity of the AKAP220-KO mice was reduced over the 30-min trial (4.1 ± 0.3 m/s; $n = 8$) compared with WT (6.3 ± 0.3 m/s; $n = 8$; Fig. 3*I*).

Open-field testing can reveal basic anxiety behaviors such as thigmotaxis, a tendency to remain close to the walls rather than exploring the open central zone of the arena (36). AKAP220-KO mice made significantly fewer excursions into the central zone during the 30-min trial (90.3 ± 9 entries; $n = 8$) compared with WT (139 ± 9.7 entries; $n = 8$; Fig. 3 *G* and *J*). In addition, the number of fecal boluses present in the arena at the completion of the trial was significantly increased for AKAP220-KO mice (Fig. 3*K*). This represents another index of anxiety (37). Parallel profiling studies

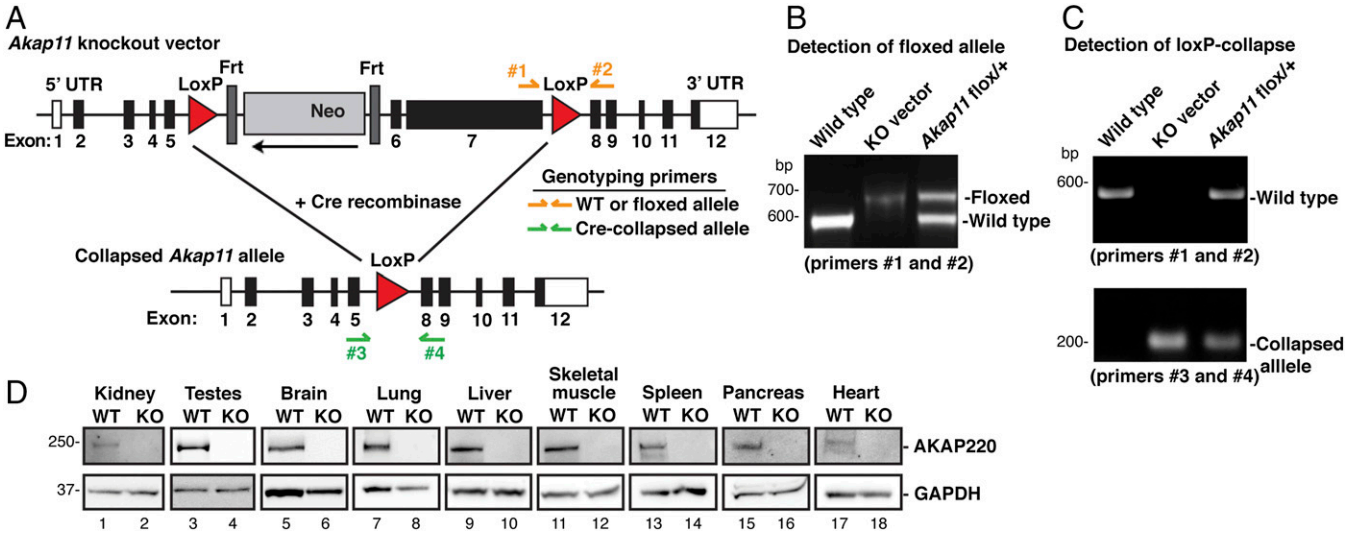

Fig. 2. Production and verification of the AKAP220-KO mouse model. (*A*) Schematic of AKAP220-KO vector shows LoxP sites flanking exons 6 and 7 of *Akap11*, the gene encoding AKAP220 (83% of coding region). An Frt-flanked neomycin (Neo) cassette and a thymidine kinase (TK) cassette were inserted as positive and negative selection markers. Genotyping primers were designed to differentiate between WT and floxed alleles (primers 1 and 2), and a separate primer pair was designed to detect the collapsed allele (primers 3 and 4). (*B*) PCR analysis with genotyping primers 1 and 2 detected the WT allele and the floxed *Akap11* allele that has a 78-bp insertion. WT DNA and purified *Akap11*-KO vector DNA were used as positive controls. (*C*) Floxed AKAP220 mice were crossed with mice expressing EIIa-Cre to generate global AKAP220-KO mice. PCR using genotyping primers 3 and 4 detected the collapsed *Akap11* allele. Two separate PCR reactions using primers 1 and 2 and primers 3 and 4 determined genotype of each animal. (*D*) Western blots show AKAP220 protein expression. (*Top*) Tissue panel from WT and AKAP220-KO mice. (*Bottom*) GAPDH was used as a loading control.

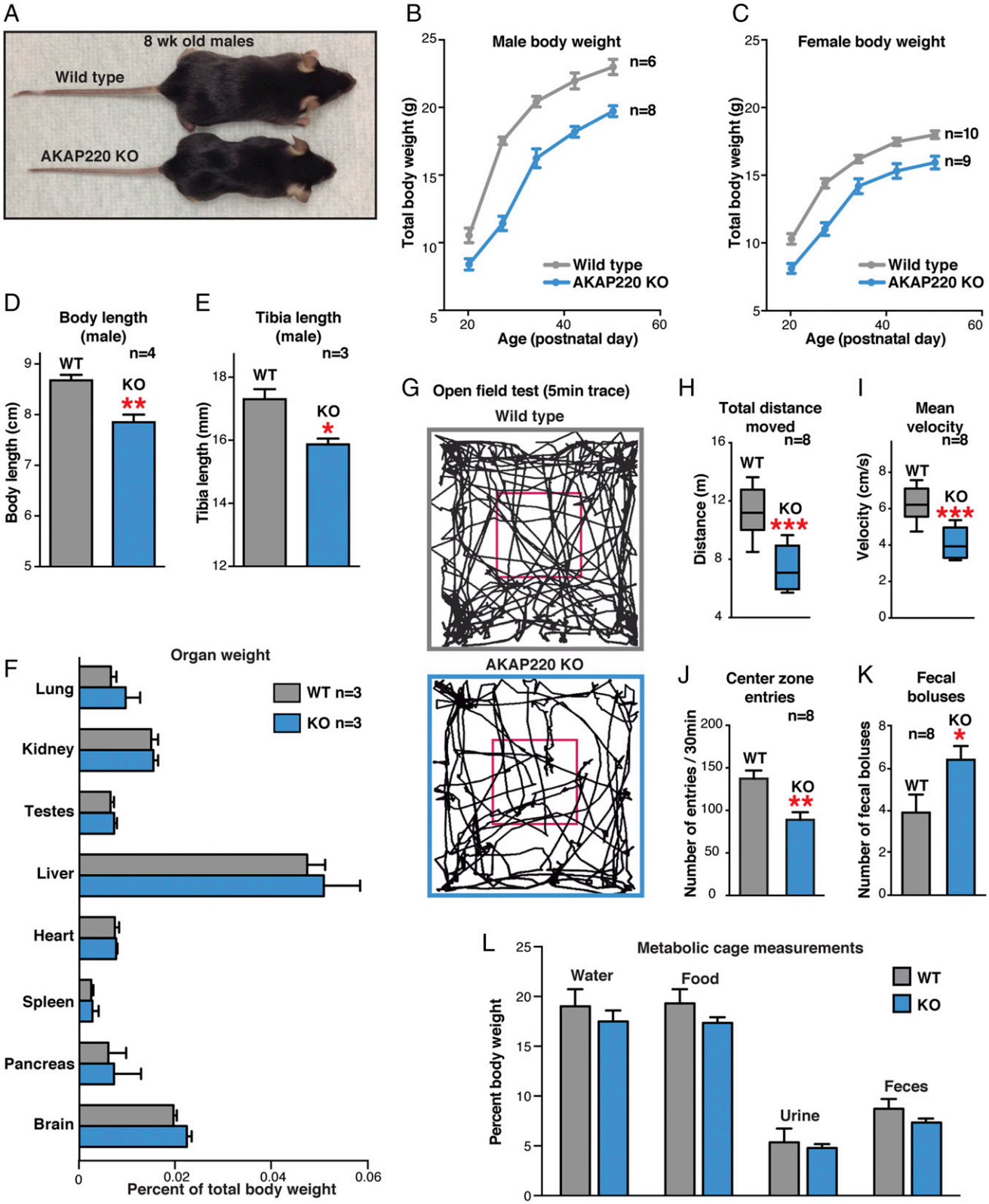

Fig. 3. AKAP220-KO mice: initial phenotypic analyses. (*A*) Photo of 8-wk postnatal WT and AKAP220-KO mice. (*B* and *C*) WT (gray) and KO (blue) total body weights from male (*B*) and female (*C*) cohorts aged 3–7 wk (*n* indicates number of animals). (*D* and *E*) Body length (nose to base of tail) and tibia length in WT (gray) and AKAP220-KO (blue) males at P50 (*n* indicates number of animals). (*F*) Relative weight of indicated organs as a percentage of total body weight for each individual animal from WT (gray) and AKAP220 KO (blue) at P50 ($n = 3$ mice per genotype). (*G–K*) Open-field test for locomotion behavior (30-min trial; $n = 8$ mice per genotype). (*G*) Representative traces of mouse movements (first 5 min). (*H* and *I*) Total distance traveled and mean velocity over 30-min trial in WT (gray) and AKAP220-KO (blue) mice. (*J* and *K*) Center zone entries (increased thigmotaxis) and fecal boluses (30-min period) for each genotype. (*L*) Metabolic cages measured daily food and water intake and urine and fecal output (measured once every 24 h for 3 d). Averages shown normalized as percentage of total body weight for each animal (8-wk-old males; $n = 4$ mice per genotype).

were initiated to establish if the reduced body size results from abnormal or reduced feeding behavior. We measured food and water intake and urine and fecal output with metabolic cages. Daily totals were recorded as the percentage of body weight. No differences were observed between WT and AKAP220-KO mice (Fig. 3*L*). These rudimentary profiling experiments show that the daily urine output of AKAP220-KO mice is normal when given free access to water. This infers that these animals do not have NDI, but does not rule out the possibility that local signaling events in the kidney that impact AQP2 apical trafficking are altered.

Apical Actin Networks Are Reduced in AKAP220-KO Kidneys. The next step was to explore the role of AKAP220 signaling elements in the modulation of actin barrier dynamics and kidney function. Because the actin barrier forms in the absence of vasopressin stimulation (13, 33), we overhydrated the animals to block vasopressin release. Animals were water-loaded by oral gavage (3% total body weight) as described previously (38). Kidneys were harvested 90 min after water loading and fixed in formalin. Paraffin-embedded kidney sections were stained with an antibody against actin (green) and counterstained with DAPI (blue) to detect nuclei (Fig. 4*A*, *Left*). Concentrated regions of actin signal are illustrated in grayscale, whereas heat-map images in pseudocolor depict signal intensity (Fig. 4*A*, *Middle* and *Right*). In WT kidney sections, a dense actin network was observed decorating the apical membranes of collecting-duct cells (Fig. 4*A*, *Upper*). This indicated that actin-barrier polymerization was intact. In contrast, apical actin enrichment was markedly reduced in kidney-collecting duct cells from AKAP220-KO mice (Fig. 4*A*, *Lower*). In fact, actin staining intensity measurements 1 μm from

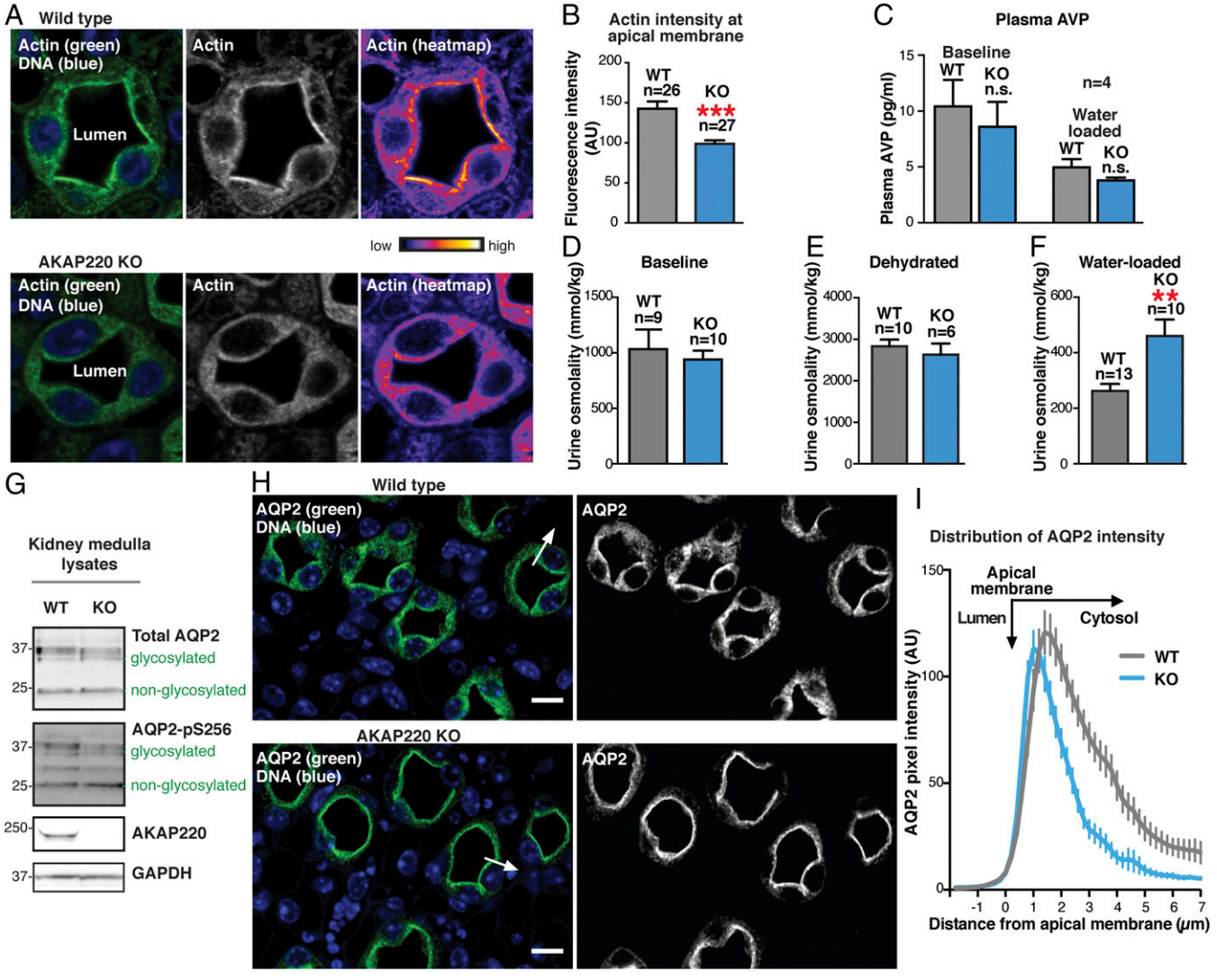

Fig. 4. Apical actin is disrupted in AKAP220-KO collecting duct cells. (*A*) Immunofluorescent staining of F-actin (green) and DNA (DAPI; blue) in kidney-collecting ducts from water-loaded WT (*Top*) and KO (*Bottom*) mice. Actin accumulation in luminal cells is shown (grayscale, *Middle*; pseudocolor heat map, *Right*). (*B*) Quantification of F-actin fluorescence intensity within 1-μm ROI of apical membranes of luminal cells. N-values and statistical significance are shown. (*C*) Plasma vasopressin (i.e., AVP) levels are shown for baseline (ad libitum water access) and water-loaded WT (gray) and AKAP220-KO (blue) mice (n = 4). (*D–F*) Urine osmolality from baseline, dehydrated (24 h), or water-loaded animals. N-values and statistical significance are shown. (*G*) Western-blot analysis of total AQP2 (*Top*) and AQP2 phospho-Ser256 (pS256-AQP2; *Upper Middle*) in kidney medulla lysates from WT and KO mice. AKAP220 (*Lower Middle*) and GAPDH (*Bottom*) are shown. Glycosylated and nonglycosylated AQP2 are indicated. (*H*, *Left*) Kidney sections from water-loaded WT and KO mice immunostained for AQP2 (green) and DNA (DAPI; blue). (Scale bar: 25 μm.) (*H*, *Right*) AQP2 immunostaining in grayscale. (*I*) AQP2 distribution along the arrow in *H* from WT (gray) and KO (blue) mice. AQP2 accumulation by line-plot analysis of fluorescence intensity. Narrowed peak indicates increased apical membrane localization.

apical membranes revealed a 30.8 ± 6% reduction in actin barrier density in AKAP220-KO kidneys ($n = 3$ mice of each genotype; $n > 26$ cells measured per replicate; Fig. 4*B*). A simple explanation for this observation could be altered release of the hormone vasopressin. Therefore, circulating plasma levels of vasopressin (i.e., AVP) in WT and AKAP220-null mice were measured by chemiluminescent immunoassay. AVP levels were not significantly different between the genotypes, indicating that vasopressin production was normal under resting conditions and appropriately inhibited upon water loading ($n = 4$; Fig. 4*C*). Thus, we can conclude that AKAP220 impacts actin barrier formation in a vasopressin-independent manner.

AKAP220 Regulates Renal Water Homeostasis. Urine is concentrated in the kidney-collecting duct when water is reabsorbed from luminal fluid (1). Because AKAP220 may regulate actin barrier formation, we reasoned that water handling might be affected in AKAP220-KO mice. To test this hypothesis, we measured urine osmolality from animals exposed to three different treatments. The baseline animals were provided ad libitum water access, the dehydrated mice were deprived of water for 24 h, and the water-loaded cohort was acutely overhydrated by oral gavage. There were no detectable differences in urine osmolality between WT and AKAP220-KO mice in the baseline and dehydrated groups ($n > 9$; Fig. 4 *D* and *E*). These studies further confirm that the vasopressin system is intact in AKAP220-KO mice, as these animals appropriately concentrate their urine in response to dehydration (Fig. 4 *D*–*F*). Conversely, in water-loaded animals, urine osmolality was 1.75-fold higher (460 ± 60 mmol/kg) in AKAP220-KO compared with WT mice (262 ± 25 mmol/kg; $P = 0.0033$, two-tailed t test; Fig. 4*F*). This indicates that AKAP220-KO mice fail to effectively respond to overhydration. On the basis of our gene-editing experiments, we reasoned that these defects in water homeostasis may relate to altered mobilization of AQP2 at the kidney-collecting duct.

Glycosylation and phosphorylation of AQP2 facilitates its membrane insertion to enhance passive water transport down an osmotic gradient (39–41). Therefore, we reasoned that the urine-osmolality phenotype in AKAP220-KO mice could result from the (*i*) overexpression of AQP2, (*ii*) changes in the glycosylation state of AQP2, or (*iii*) changes in the phosphorylation status of the water pore. Western blot analysis of kidney medulla extracts by using an antibody that recognizes total AQP2 detected equivalent levels of the glycosylated and nonglycosylated forms of the water pore in samples from both genotypes ($n > 4$ for each genotype; Fig. 4*G*, *Top*). Control immunoblots confirmed loss of AKAP220 and equal loading by GAPDH (Fig. 4*G*, *Middle* and *Bottom*). As previously stated, PKA phosphorylation of serine 256 on AQP2 enhances water permeability in the collecting duct. Immunoblot analysis using phosphopeptide-specific antibodies detected equivalent levels of p-Ser256 AQP2 in medulla extracts from both genotypes (Fig. 4*G*, *Upper Middle*). Unfortunately, antibodies used to evaluate the baseline phosphorylation state of AQP2 were no longer available when we were ready to evaluate p-Ser256 AQP2 levels in medulla extracts from water-loaded mice of either genotype. Nevertheless, the loss of AKAP220 did not alter protein expression, glycosylation, or phosphorylation of AQP2 on Ser256.

AQP2 Accumulation at the Apical Surfaces of AKAP220-KO Collecting Ducts. As no changes in the expression levels or covalent modification of AQP2 were evident in AKAP220-KO mice, a logical next step was to determine whether actin-barrier defects influence the subcellular location of the water pore. Paraffin-embedded kidney sections from water-loaded animals were immunolabeled with an anti-AQP2 antibody (green) and counterstained with DAPI (blue) to identify nuclei (Fig. 4*H*, *Left*). In WT tissue, AQP2 was observed to have punctate cytosolic, perinuclear, and apical membrane localization that was restricted to the principal cells of the collecting duct (Fig. 4*H*, *Upper*). This is characteristic of an overhydrated animal when the water pore is internalized into vesicles to prevent water reabsorption (42, 43).

Conversely, in kidney sections from AKAP220-KO mice, the AQP2 signal was restricted to the apical membrane of cells lining the lumen (Fig. 4*H*, *Bottom*). Quantification by line-plot analysis of pixel intensity (Fig. 4*H*, *Left*, arrow) revealed a shift of AQP2 distribution toward the apical membranes ($n \geq 52$ cells; $n = 3$ replicates; representative technical replicate shown in Fig. 4*I*). This AQP2 redistribution is consistent with the observed urine osmolality phenotype of AKAP220-KO mice. Under this scenario, water reabsorption would continue upon overhydration as AQP2 persists on the apical membrane of the collecting duct cells.

Altered RhoA Localization and Activity in AKAP220-KO Kidneys. Dynamic and reversible remodeling of the apical F-actin barrier has been linked to AQP2 trafficking to the apical membrane (13, 44). Moreover, AKAP220 complexes have been shown to regulate cytoskeletal remodeling by anchoring PKA, GSK3β, and IQGAPs at the cortical actin network (27, 28). For these reasons, we wanted to examine whether the apical membrane accumulation of AQP2 in AKAP220-KO kidneys could be caused by actin-barrier defects. Previous studies have implicated the small GTPase RhoA as a molecular switch that triggers actin barrier polymerization (15). Paraffin-embedded kidney sections from WT and AKAP220-KO mice were immunostained with antibodies to RhoA (Fig. 5*A*, red) and AQP2 (Fig. 5*A*, green). In WT sections, the RhoA signal was predominantly cytoplasmic and overlapped with AQP2 (Fig. 5*A*, *Top*). Interestingly, in AKAP220-KO sections, RhoA and AQP2 exhibited more restricted and apical staining patterns in the principal cells of the collecting ducts (Fig. 5*A*, *Bottom*). Line-plot analysis of RhoA fluorescence intensity confirmed a redistribution of RhoA signal toward the apical membrane in AKAP220-KO tissue compared with WT ($n \geq 49$ cells; $n = 3$ replicates; representative technical replicate shown in Fig. 5*B*). Surprisingly, these data suggest that RhoA and AQP2 may be functionally coupled and, in some way, contribute to the AKAP220-KO phenotype. That being said, the molecular details of this functional interface remain unclear. Technical issues precluded any definitive analysis of whether RhoA is recruited directly to the AKAP220 signaling complex. For example, immunoblot detection of Rho within AKAP220 immune complexes was obscured by the heavy/light chains of our custom AKAP220 antibody. Further studies and the development of additional reagents will be needed to explore the mode of interaction between AKAP220 and RhoA.

More mechanistic studies monitored GTP-RhoA levels as an index of cellular GTPase activity. Kidney medullas were harvested from baseline and water-loaded mice. Tissues lysates were combined with agarose beads conjugated to the Rho-binding domain of Rhotekin to pull down active, GTP-bound RhoA. Immunoblot analysis was used to compare total RhoA to the GTP loaded and active form of the GTPase ($n = 8$; Fig. 5 *C* and *D*). At baseline conditions, the levels of GTP-RhoA were similar in samples from both genotypes (Fig. 5*C*). However, after water loading, GTP-RhoA levels were reduced in medullar extracts from AKAP220-KO mice compared with WT (Fig. 5*D*). Quantification of the amalgamated data from six pull-down experiments revealed a significant decrease in GTP-RhoA/total RhoA ratios from water-loaded AKAP220-KO mice compared with WT (Fig. 5*E*). Therefore, this reduction in RhoA activity could inhibit actin barrier polymerization and permit membrane accumulation of AQP2 in the collecting ducts of AKAP220-null mice. Together, these studies identify a role of AKAP220 signaling complexes in actin barrier maintenance, AQP2 trafficking, and body water homeostasis.

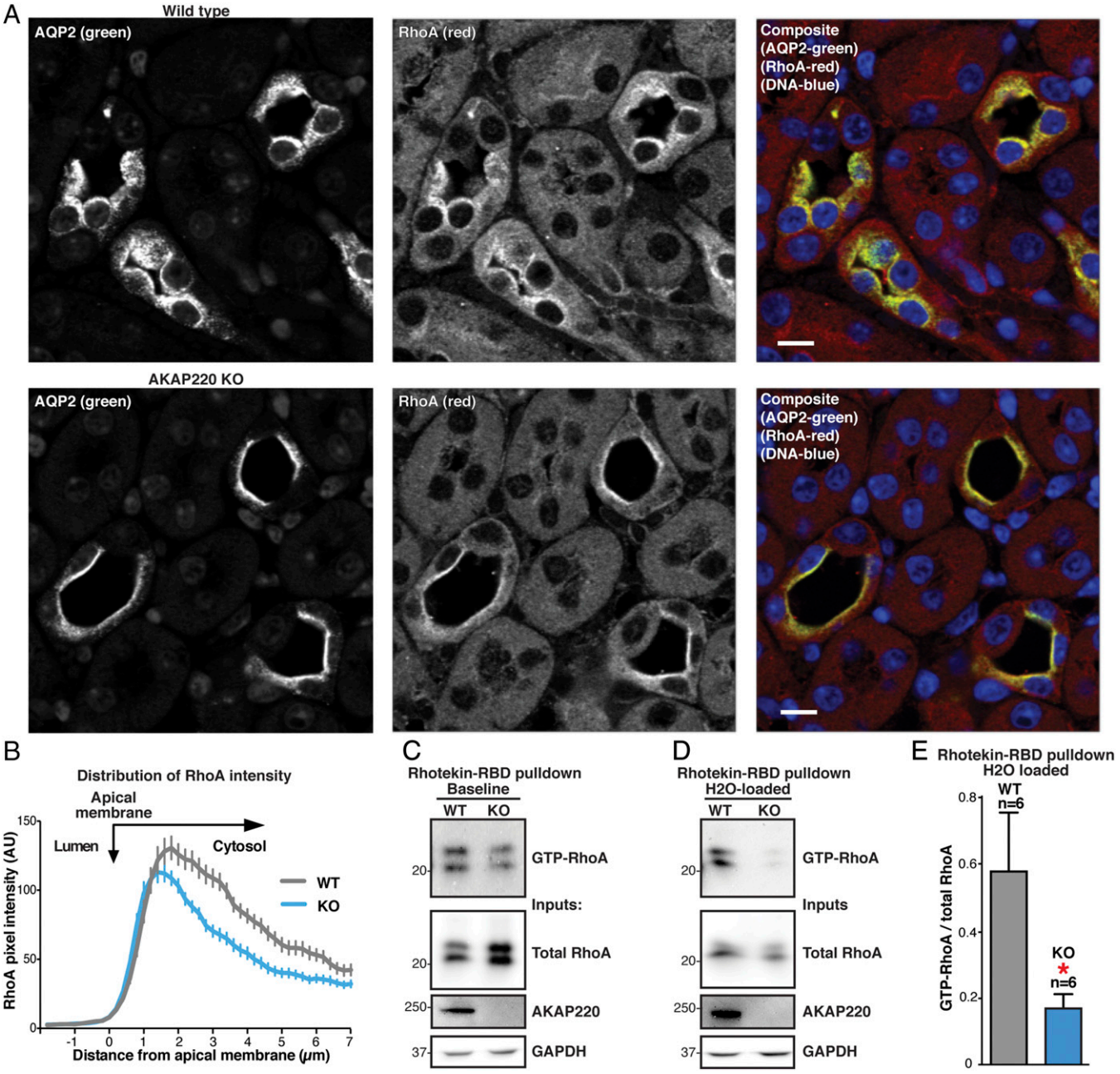

Fig. 5. AKAP220-KO kidneys have decreased active, GTP-bound RhoA. (*A*) Immunostaining of kidney sections from water-loaded WT (*Top*) and AKAP220-KO (*Bottom*) mice to detect AQP2 (*Left*) and RhoA (*Middle*) in composite with DNA (DAPI; blue). (Scale bar: 25 μm.) (*B*) Line-plot analysis of RhoA fluorescence intensity in *A* along a line from the interior of the lumen, across the apical membrane, and into the cytoplasm of the luminal cells. Traces from WT (gray) and AKAP220-KO (blue) sections were quantified. A more narrowed peak is indicative of increased apical membrane localization. Distance from the edge of the apical membrane is measured in microns. (*C* and *D*) Rhotekin-RBD beads were used to isolate GTP-bound RhoA from animals given ad libitum water access (baseline; *C*) and water-loaded animals (*D*). (*Top*) Western-blot analysis of GTP-RhoA levels in kidney medulla lysates from WT (lane 1) and AKAP220-KO animals (lane 2). Total RhoA (*Upper Middle*), AKAP220 (*Lower Middle*), and GAPDH controls (*Bottom*) are shown. (*E*) Quantification of amalgamated data from six Rhotekin-RBD pull-downs. Inputs and pull-downs were run on the same blot and probed for RhoA. Signal intensity for GTP-RhoA (pull-down) was measured and normalized to total RhoA (input) for each sample. AKAP220-KO samples had a significantly lower ratio of GTP-RhoA to total RhoA ($P = 0.047$, two-tailed Student *t* test).

Discussion

Appropriate hydration is essential to preserve plasma volume, electrolyte balance, and intercellular osmolarity. In mammals, the principal effector organ is the kidney, where a variety of endocrine factors influence water homeostasis. Prolonged water deprivation or excessive sweating leads to dehydration. This triggers release of the pituitary hormone vasopressin, which in turn stimulates cAMP-responsive membrane insertion of the AQP2 water pore into cells lining the kidney collecting duct (5). The net effect is to promote renal water reabsorption. Although most research has focused on the covalent modification and membrane trafficking of AQP2 as an endocrine response to dehydration, less is known about how AQP2-containing vesicles are managed when circulating vasopressin levels are low. Thus,

additional signals must govern AQP2 movement in a hormone-independent manner. Under basal conditions, a dense network of apical F-actin, termed the actin barrier, impedes fusion of AQP2-containing vesicles (15). Maintenance and remodeling of this cytoskeletal structure involves small molecular weight GTPases (13). Consequently, understanding the local signaling events that manage actin barrier dynamics is an important and underappreciated aspect of water homeostasis. In this study, we define a new role for AKAP220 signaling complexes in the vasopressin-independent regulation of actin-barrier dynamics and the subcellular localization of AQP2 in the kidney.

AKAPs have previously been implicated in the hormonal control of AQP2 phosphorylation (22, 45). AKAP18δ is a known constituent of AQP2-containing vesicles, where it may anchor PKA to promote vasopressin responsive phosphorylation of the water pore (19, 21, 22). Others have identified an AKAP-associated pool of the phosphatase PP2B that is thought to dephosphorylate AQP2 at the apical membranes of the inner medullary-collecting duct (30). In addition, an anchoring protein in excess of 200 kDa cofractionates with endosomes from these cells (20). Although this high molecular weight RII-binding protein was initially thought to be AKAP-Lbc, subsequent studies have shown that this anchoring protein is sparingly expressed in the kidney and does not associate with AQP2-containing vesicles (20, 46, 47). Hence, we now propose that the enigmatic vesicular anchoring protein is AKAP220. Our evidence that loss of AKAP220 elicits defects in actin dynamics when combined with reports of a physical association between this anchoring protein and the water channel (22) allow us to postulate that a macromolecular complex of AKAP220, its binding partners, and AQP2 enables precise and local control of renal water homeostasis.

To test our hypothesis in a physiological context, we generated AKAP220-KO mice. Our strategy was to cross the LoxP-AKAP220 line with mice expressing Cre recombinase under the control of the adenovirus EIIa promoter. This generated a preimplantation, early embryonic KO of AKAP220 that does not affect the vasopressin regulatory axis. We reasoned that this strategy was preferable to the more involved process of producing a kidney-specific KO, as it may reveal other overt phenotypes outside the kidney. Indeed, our initial characterization of these animals revealed a reduced body size that persists throughout life, yet the daily food and water intake of these animals was comparable to those of WT mice (Fig. 3). When evaluated in the open-field test, AKAP220-KO mice exhibited reduced motility and increased thigmotaxis. These initial findings point toward an anxiety phenotype that ultimately warrants further investigation. However, our intent was to study the role of AKAP220 in renal function. To this end, we detected actin-barrier defects first in AKAP220$^{-/-}$ mIMCD3 spheroids and then in principal cells of the kidney-collecting ducts from AKAP220-null mice (Figs. 1 and 4). An important outcome of impaired actin-barrier formation is the overaccumulation of AQP2 at the apical surface of collecting ducts (Fig. 4). This ultimately promotes stress-induced changes in water handling, as AKAP220-null mice excrete urine with abnormally high osmolality when overhydrated.

Mechanistic investigation of AKAP220 signaling to the apical actin network demonstrated that active, GTP-bound RhoA is reduced in medullar extracts from AKAP220-KO mice (Fig. 5). This allows us to propose that mislocalization and attenuation of Rho signaling negatively impacts apical actin remodeling and maintenance of the actin barrier. Indirect support for this hypothesis comes from studies showing that pharmacological inhibition of Rho family GTPases causes accumulation of AQP2 at the apical membrane in the absence of vasopressin (15, 19, 44). Therefore, we conclude that AKAP220 coordinates a macromolecular complex of signaling enzymes and effector proteins that direct AQP2 localization and promote water excretion. One key element of this signaling complex is likely to be the Rho-family GTPase effector protein IQGAP (27, 28). We have previously shown that AKAP220 sequesters IQGAPs near the cell cortex to positively regulate actin polymerization and microtubule stability during membrane protrusion and cell migration (27, 28). These processes are reminiscent of the actin-barrier phenotypes we observed in kidney collecting ducts of AKAP220-KO mice. Two in situ approaches support this concept. Gene editing of AKAP220 in mIMCD3 cells disrupted apical F-actin networks in polarized 3D cultures (Fig. 1). Additionally, immunoblot profiling experiments confirm that AKAP220 ancillary proteins such as IQGAP1 and RhoA are present at normal levels in cells lacking this anchoring protein (Fig. 1). Thus, loss of AKAP220 promotes the cellular redistribution of its binding partners, rather than altering the expression levels of these proteins.

Another interesting facet of our work is that the phosphorylation status of AQP2 is unaltered in our KO mice. Paradoxically, this infers that AKAP220-associated pools of PKA are not essential for this aspect of AQP2 physiology. Several factors corroborate this notion. It is widely accepted that PKA phosphorylation of Ser256 on AQP2 occurs in response to endocrine release of vasopressin (5), yet the data in Figs. 4 and 5 definitively exclude a role for this hormone in the AKAP220-KO phenotype. Consequently, PKA phosphorylation events that augment AQP2 pore function must proceed through other AKAP-associated pools of this kinase. Likely candidates include AKAP18δ, a PKA-anchoring protein that codistributes, but does not interact with, AQP2, and AKAP79/150 that tethers PKA to membrane-proximal regions (48–51). There is clear precedent for AKAPs that participate in PKA-independent signaling events. Notable examples include (*i*) protein kinase D-mediated nuclear export of histone deacetylases in cardiomyocytes (47), (*ii*) organization of ubiquitin ligases that facilitate the proteosomal degradation of HIF1a at the nuclear pore (52), and (*iii*) synchronization of Rac GTPases with the Arp2/3 complex during dendritic actin-remodeling events (53). Thus, our discovery that AKAP220 sequesters RhoA to modulate the apical actin barrier in kidney-collecting duct cells is an important addition to our understanding of the versatility of AKAPs as physiological effectors of local signaling processes (18, 54).

Finally, our studies detail a broadly based, in vivo investigation of AKAP220 function. Loss of AKAP220 leads to accumulation of AQP2 at the plasma membrane and reduces urine-diluting capacity during overhydration. This phenotype is clinically relevant, as increasing AQP2 at the apical membrane is the desired therapeutic outcome when treating patients with NDI (8, 55). Current treatment options for patients with congenital NDI are limited and relatively ineffective (2). Hence, elucidating the signaling pathways disrupted in AKAP220-KO mice could reveal new pharmacological targets for this disease. Because most cases of congenital NDI are caused by mutations in the V2R, pharmacologically reengaging the signaling elements downstream of this receptor could restore AQP2 trafficking. Therefore, our discovery that AKAP220 signaling complexes influence RhoA-dependent AQP2 localization provides important insight toward much needed therapeutic avenues for NDI treatment.

Methods

Knockout Vector. The KO vector was generated using a Bacmid (Children's Hospital Oakland Research Institute, clone RP23-239B21). Vega Biolabs engineered a retrieval plasmid containing arms of homology flanking the target sequence to capture ~14 kb of genomic *Akap11* locus. LoxP sites were added to intronic regions surrounding exons 6 and 7 and a Neo cassette flanked by two Frt sites (removed by breeding with mice expressing FLP recombinase). *HSV-TK*I cassette served as negative selection marker (outside the *Akap11* genomic sequence). ES cell clones were grown in the presence of

fialuridine. Southern blot band shift identified incorporation of BamHI and StuI sites into genomic DNA.

ES Cell Electroporation. KO vector was digested overnight (37 °C) with the I-CeuI recognition sequence (5′-TAACTATAACGGTCCTAA^GGTAGCGAA-3′, occurs only once in the KO vector, outside the captured *Akap11* genomic region). G4 hybrid ES cells (129S6/SvEvTac and C57BL/6Ncr cross; University of Washington Transgenics Resources Program) were electroporated and grown under selection by G418 for incorporation of Neo cassette.

ES Cell Screening. DNA was purified from ES cells and screened for homologous recombination: PCR primers designed to flank the 3′ loxP site (forward primer, 5′-GACAAATGCTGGGCATGCTGTTAGCAGG-3′; reverse primer, 5′-CAAGCTTAA-GGAAGACTGCGGGGTAC-3′). WT sequence produces a 579-bp PCR product, whereas a loxP site between the primers creates a 657-bp product. The StuI site provided confirmation of PCR products by restriction digest. Positive PCR clones were then digested with BamHI or StuI and screened by Southern blot.

Chimera Production. ES cells were microinjected into C57BL/6J blastocysts and implanted into pseudopregnant mice. Agouti coat identified chimeric offspring before breeding with C57BL/6J and PCR validation of germ-line transmission of loxed*Akap11* allele. This study was performed in strict accordance with the recommendations in the *Guide for the Care and Use of Laboratory Animals* of the National Institutes of Health (56). All of the animals were handled according to approved Institutional Animal Care and Use Committee (IACUC) protocols (#4196-01) of the University of Washington.

FRT-FLP and Cre-lox Breeding. Crossing with mice expressing FLP recombinase [B6(C3)-Tg(Pgk1-FLPo)10Sykr/J] removed the Frt-flanked Neo cassette. After deletion of the Neo cassette was confirmed, KO mice were produced by crossing *Akap11*$^{lox/lox}$ animals with mice expressing Cre recombinase. Offspring were screened for the Cre transgene and the WT, floxed, or collapsed *Akap11* alleles.

Genotyping. Genotyping the floxed*Akap11* allele was done with primers used in ES cell screening. A second PCR primer pair annealing outside the loxP sites detected loxP collapse in *Akap11*$^{-/-}$ mice. Full genotyping of global KO animals requires the WT and collapsed PCR reactions. Heterozygous animals have PCR products present in both reactions, whereas homozygotes are positive for only the WT or collapsed allele.

Metabolic Cages. Mice housed individually in Tecniplast metabolic cages were provided mash/crumble LabDiet 5053 and acclimatized for 4 d before testing. The water bottle, food hopper, and urine and feces collection cups from each cage were weighed every 24 h for 3 d.

Open-Field Test. Open-field test was conducted as previously described (34, 35). Before each trial, boxes were cleaned with 70% ethanol. Age-matched male mice were recorded for 30 min, and videos were analyzed for animal movement, velocity, and number of entries into the central zone (EthoVision 3.0).

Tissue Lysis. Kidneys tissue was lysed in ice-cold RIPA buffer (50 mM Tris·HCl, pH 8.0, 150 mM NaCl, 1% Nonidet P-40, 0.5% sodium deoxycholate, 0.1% SDS, protease inhibitor mixture) using a BioVortexer (RPI).

Dehydration and Water Loading (Overhydration). For dehydration, water access was removed for 24 h. For water loading, oral gavage with 10% (vol/vol) glucose in water (3% total body weight) was followed by a 30-min recovery before urine collection. Before treatment, mice were scruffed to void bladder and ensure that collection cage samples were representative of a water-loaded state.

Urine Osmolality. Urine samples were collected using individual boxes lined with 96-well plates. Osmolality was measured using Vapro vapor pressure osmometer (model 5520) calibrated with Wescor Opti-Mole standards.

Tissue Staining. Kidneys were fixed in 10% (vol/vol) buffered formalin (4 °C), embedded in paraffin and 4-μm-thick sections collected. Sections were deparaffinized (Citrasolv; Fisher), antigen retrieved (buffer A, Retriever 2100 pressure cooker; Electron Microscopy Sciences), and tissue sections blocked in 10% (vol/vol) donkey serum/PBS solution before incubation with antibodies.

Line-Plot Analysis. Protein localization was assessed by line-plot analysis of pixel intensity (ImageJ).

Rhotekin Pull-Down Assay. Rhotekin pull-down assay was performed by using kidney lysates according to the manufacturer's instructions (Cytoskeleton).

mIMCD3 Spheroid. Spheroids were formed as previously described (31). Actin and DNA were stained with fluorescent phalloidin and DRAQ5 before spinning-disk confocal analysis of spheroids with visible, open lumen.

AVP Chemiluminescent Immunoassay. Vasopressin concentration was measured by using the Arg^{8}-Vasopressin Chemiluminescent Immunoassay kit (Arbor Assays).

Antibodies Used.

Actin. 1) Mouse monoclonal anti–β-actin (cat. no. A3853; Sigma) was used in Western blots at a 1:10,000 dilution. 2) ActinGreen 488 ReadyProbes Reagent (cat. no. R37110; Thermo Fisher), was used according to the manufacturer's instructions (2 drops/milliliter).

PKA (catalytic subunit). Mouse monoclonal anti-PKAc (cat. no. 610981; BD Biosciences), was used in Western blot at 1:5,000 dilution.

IQGAP. Mouse monoclonal anti-IQGAP1 (cat. no. 33–8900; Invitrogen), was used in Western blot at 1:3,000 dilution.

GAPDH. Mouse monoclonal anti-GAPDH (cat. no. G9295; Sigma), was used in Western blot at 1:3,000 dilution.

AKAP220. Custom rabbit polyclonal anti-AKAP220, was used in Western blot at 1:3,000 dilution.

RhoA. Rabbit polyclonal anti-RhoA (cat. no. sc-179; Santa Cruz), was used in Western blot at 1:1,000 dilution.

RhoA. Mouse monoclonal anti-RhoA (cat. no. sc-418; Santa Cruz), was used in immunostaining at 1:500 dilution.

AQP2. Rabbit polyclonal anti-AQP2 (cat. no. ab15116; Abcam), was used in Western blots at 1:2,000 dilution and in immunostaining at 1:400 dilution.

pS256-AQP2. Rabbit polyclonal anti-AQP2-pS256 (from the laboratory of Mark Knepper, Epithelial Systems Biology Laboratory, National Heart, Lung, and Blood Institute, Bethesda), was used in Western blots at 1:1,000 dilution.

ACKNOWLEDGMENTS. The authors thank F. Donelson Smith for his assistance with critical review and experimental design and Merle L. Gilbert for helpful discussions. This work was supported by National Institutes of Health Grants DK105542 and DK054441 (to J.D.S).

1. Saborio P, Tipton GA, Chan JC (2000) Diabetes insipidus. *Pediatr Rev* 21:122–129, quiz 129.
2. Noda Y, Sohara E, Ohta E, Sasaki S (2010) Aquaporins in kidney pathophysiology. *Nat Rev Nephrol* 6(3):168–178.
3. Bankir L, Bouby N, Ritz E (2013) Vasopressin: A novel target for the prevention and retardation of kidney disease? *Nat Rev Nephrol* 9(4):223–239.
4. Yui N, Lu HJ, Bouley R, Brown D (2012) AQP2 is necessary for vasopressin- and forskolin-mediated filamentous actin depolymerization in renal epithelial cells. *Biol Open* 1(2):101–108.
5. King LS, Kozono D, Agre P (2004) From structure to disease: The evolving tale of aquaporin biology. *Nat Rev Mol Cell Biol* 5(9):687–698.
6. Canfield MC, Tamarappoo BK, Moses AM, Verkman AS, Holtzman EJ (1997) Identification and characterization of aquaporin-2 water channel mutations causing nephrogenic diabetes insipidus with partial vasopressin response. *Hum Mol Genet* 6(11):1865–1871.
7. Pasel K, et al. (2000) Functional characterization of the molecular defects causing nephrogenic diabetes insipidus in eight families. *J Clin Endocrinol Metab* 85(4): 1703–1710.
8. van Lieburg AF, et al. (1994) Patients with autosomal nephrogenic diabetes insipidus homozygous for mutations in the aquaporin 2 water-channel gene. *Am J Hum Genet* 55(4):648–652.
9. Iolascon A, et al. (2007) Characterization of two novel missense mutations in the AQP2 gene causing nephrogenic diabetes insipidus. *Nephron Physiol* 105(3): 33–41.
10. Yang B, Zhao D, Verkman AS (2009) Hsp90 inhibitor partially corrects nephrogenic diabetes insipidus in a conditional knock-in mouse model of aquaporin-2 mutation. *FASEB J* 23(2):503–512.
11. Yun J, et al. (2000) Generation and phenotype of mice harboring a nonsense mutation in the V2 vasopressin receptor gene. *J Clin Invest* 106(11):1361–1371.
12. Promeneur D, Kwon TH, Frøkiaer J, Knepper MA, Nielsen S (2000) Vasopressin V(2)-receptor-dependent regulation of AQP2 expression in Brattleboro rats. *Am J Physiol Renal Physiol* 279(2):F370–F382.
13. Simon H, Gao Y, Franki N, Hays RM (1993) Vasopressin depolymerizes apical F-actin in rat inner medullary collecting duct. *Am J Physiol* 265(3 pt 1):C757–C762.

14. Klussmann E, et al. (2001) An inhibitory role of Rho in the vasopressin-mediated translocation of aquaporin-2 into cell membranes of renal principal cells. *J Biol Chem* 276(23):20451–20457.
15. Tamma G, et al. (2003) cAMP-induced AQP2 translocation is associated with RhoA inhibition through RhoA phosphorylation and interaction with RhoGDI. *J Cell Sci* 116(pt 8):1519–1525.
16. Tamma G, et al. (2005) Actin remodeling requires ERM function to facilitate AQP2 apical targeting. *J Cell Sci* 118(Pt 16):3623–3630.
17. Sim AT, Scott JD (1999) Targeting of PKA, PKC and protein phosphatases to cellular microdomains. *Cell Calcium* 26(5):209–217.
18. Langeberg LK, Scott JD (2015) Signalling scaffolds and local organization of cellular behaviour. *Nat Rev Mol Cell Biol* 16(4):232–244.
19. Klussmann E, Rosenthal W (2001) Role and identification of protein kinase A anchoring proteins in vasopressin-mediated aquaporin-2 translocation. *Kidney Int* 60(2): 446–449.
20. Klussmann E, et al. (2001) Ht31: The first protein kinase A anchoring protein to integrate protein kinase A and Rho signaling. *FEBS Lett* 507(3):264–268.
21. Henn V, et al. (2004) Identification of a novel A-kinase anchoring protein 18 isoform and evidence for its role in the vasopressin-induced aquaporin-2 shuttle in renal principal cells. *J Biol Chem* 279(25):26654–26665.
22. Okutsu R, et al. (2008) AKAP220 colocalizes with AQP2 in the inner medullary collecting ducts. *Kidney Int* 74(11):1429–1433.
23. Lester LB, Coghlan VM, Nauert B, Scott JD (1996) Cloning and characterization of a novel A-kinase anchoring protein. AKAP 220, association with testicular peroxisomes. *J Biol Chem* 271(16):9460–9465.
24. Tanji C, et al. (2002) A-kinase anchoring protein AKAP220 binds to glycogen synthase kinase-3beta (GSK-3beta) and mediates protein kinase A-dependent inhibition of GSK-3beta. *J Biol Chem* 277(40):36955–36961.
25. Schillace RV, Scott JD (1999) Association of the type 1 protein phosphatase PP1 with the A-kinase anchoring protein AKAP220. *Curr Biol* 9(6):321–324.
26. Whiting JL, et al. (2015) Protein Kinase A Opposes the Phosphorylation-dependent Recruitment of Glycogen Synthase Kinase 3β to A-kinase Anchoring Protein 220. *J Biol Chem* 290(32):19445–19457.
27. Logue JS, et al. (2011) AKAP220 protein organizes signaling elements that impact cell migration. *J Biol Chem* 286(45):39269–39281.
28. Logue JS, Whiting JL, Scott JD (2011) Sequestering Rac with PKA confers cAMP control of cytoskeletal remodeling. *Small GTPases* 2(3):173–176.
29. Uawithya P, Pisitkun T, Ruttenberg BE, Knepper MA (2008) Transcriptional profiling of native inner medullary collecting duct cells from rat kidney. *Physiol Genomics* 32(2):229–253.
30. Jo I, et al. (2001) AQP2 is a substrate for endogenous PP2B activity within an inner medullary AKAP-signaling complex. *Am J Physiol Renal Physiol* 281(5):F958–F965.
31. Giles RH, Ajzenberg H, Jackson PK (2014) 3D spheroid model of mIMCD3 cells for studying ciliopathies and renal epithelial disorders. *Nat Protoc* 9(12):2725–2731.
32. Hehnly H, et al. (2015) A mitotic kinase scaffold depleted in testicular seminomas impacts spindle orientation in germ line stem cells. *eLife* 4:e09384.
33. Loo CS, et al. (2013) Quantitative apical membrane proteomics reveals vasopressin-induced actin dynamics in collecting duct cells. *Proc Natl Acad Sci USA* 110(42): 17119–17124.
34. Christmas AJ, Maxwell DR (1970) A comparison of the effects of some benzodiazepines and other drugs on aggressive and exploratory behaviour in mice and rats. *Neuropharmacology* 9(1):17–29.
35. Whimbey AE, Denenberg VH (1967) Two independent behavioral dimensions in open-field performance. *J Comp Physiol Psychol* 63(3):500–504.
36. Simon P, Dupuis R, Costentin J (1994) Thigmotaxis as an index of anxiety in mice. Influence of dopaminergic transmissions. *Behav Brain Res* 61(1):59–64.
37. Walsh RN, Cummins RA (1976) The Open-Field Test: A critical review. *Psychol Bull* 83(3):482–504.
38. Rieg T, et al. (2010) Adenylate cyclase 6 determines cAMP formation and aquaporin-2 phosphorylation and trafficking in inner medulla. *J Am Soc Nephrol* 21(12): 2059–2068.
39. Fushimi K, Sasaki S, Marumo F (1997) Phosphorylation of serine 256 is required for cAMP-dependent regulatory exocytosis of the aquaporin-2 water channel. *J Biol Chem* 272(23):14800–14804.
40. Nishimoto G, et al. (1999) Arginine vasopressin stimulates phosphorylation of aquaporin-2 in rat renal tissue. *Am J Physiol* 276(2 pt 2):F254–F259.
41. Nielsen S, Muller J, Knepper MA (1993) Vasopressin- and cAMP-induced changes in ultrastructure of isolated perfused inner medullary collecting ducts. *Am J Physiol* 265(2 Pt 2):F225–F238.
42. Noda Y, Sasaki S (2005) Trafficking mechanism of water channel aquaporin-2. *Biol Cell* 97(12):885–892.
43. Brown D (2003) The ins and outs of aquaporin-2 trafficking. *Am J Physiol Renal Physiol* 284(5):F893–F901.
44. Tamma G, et al. (2001) Rho inhibits cAMP-induced translocation of aquaporin-2 into the apical membrane of renal cells. *Am J Physiol Renal Physiol* 281(6):F1092–F1101.
45. Klussmann E, Maric K, Wiesner B, Beyermann M, Rosenthal W (1999) Protein kinase A anchoring proteins are required for vasopressin-mediated translocation of aquaporin-2 into cell membranes of renal principal cells. *J Biol Chem* 274(8):4934–4938.
46. Diviani D, Soderling J, Scott JD (2001) AKAP-Lbc anchors protein kinase A and nucleates Galpha 12-selective Rho-mediated stress fiber formation. *J Biol Chem* 276(47): 44247–44257.
47. Carnegie GK, et al. (2008) AKAP-Lbc mobilizes a cardiac hypertrophy signaling pathway. *Mol Cell* 32(2):169–179.
48. Sanderson JL, Dell'Acqua ML (2011) AKAP signaling complexes in regulation of excitatory synaptic plasticity. *Neuroscientist* 17:321–336.
49. Brandon NJ, et al. (2003) A-kinase anchoring protein 79/150 facilitates the phosphorylation of GABA(A) receptors by cAMP-dependent protein kinase via selective interaction with receptor beta subunits. *Mol Cell Neurosci* 22(1):87–97.
50. Snyder EM, et al. (2005) Role for A kinase-anchoring proteins (AKAPS) in glutamate receptor trafficking and long term synaptic depression. *J Biol Chem* 280(17):16962–16968.
51. Tunquist BJ, et al. (2008) Loss of AKAP150 perturbs distinct neuronal processes in mice. *Proc Natl Acad Sci USA* 105(34):12557–12562.
52. Wong W, Goehring AS, Kapiloff MS, Langeberg LK, Scott JD (2008) mAKAP compartmentalizes oxygen-dependent control of HIF-1alpha. *Sci Signal* 1(51):ra18.
53. Soderling SH, et al. (2002) The WRP component of the WAVE-1 complex attenuates Rac-mediated signalling. *Nat Cell Biol* 4(12):970–975.
54. Smith FD, et al. (2010) AKAP-Lbc enhances cyclic AMP control of the ERK1/2 cascade. *Nat Cell Biol* 12(12):1242–1249.
55. Morello JP, Bichet DG (2001) Nephrogenic diabetes insipidus. *Annu Rev Physiol* 63: 607–630.
56. Committee on Care and Use of Laboratory Animals (1996) *Guide for the Care and Use of Laboratory Animals* (Natl Inst Health, Bethesda), DHHS Publ No (NIH) 85–23.